International Communications in Heat and Mass Transfer 175 (2026) 111192

Contents lists available at ScienceDirect

International Communications in Heat and Mass Transfer

journal homepage: www.elsevier.com/locate/ichmt

Multiphysics simulation of laser tattoo removal and prediction of required sessions: Effects of fluence, ink concentration, and tattooed dermal thickness

Vannakorn Mongkol [a], Wutipong Preechaphonkul [b], Suphak Khumsupha [a], Kittipong Junsook [a], Phadungsak Rattanadecho [a,*]

[a] Hub of Talents Electromagnetic Energy Utilization in Medical Engineering, Department of Mechanical Engineering, Faculty of Engineering, Thammasat University (Rangsit Campus), Khlong Luang, Pathum Thani 12120, Thailand
[b] Institute of field robotics, King Mongkut's University of Technology Thonburi, Bangkok, Thailand

ARTICLE INFO

Keywords:
Laser
Tattoo
Biological skin
Bioheat
Multiphysics modeling
Numerical analysis
Simulation

ABSTRACT

Laser tattoo removal is a widely adopted clinical procedure due to its precision and minimal invasiveness; however, predicting the required number of treatment sessions remains a major challenge. This study developed a numerical Multiphysics model to predict the number of sessions necessary for effective tattoo removal, providing a systematic and quantitative approach to optimize treatment parameters. The model integrates light transport, bioheat transfer, and mass transfer equations to simulate temperature distribution, optical absorption, and ink concentration in multilayered skin tissue. Numerical simulations were conducted in COMSOL Multiphysics using a 1064 nm laser at fluences of 0.3–6 J/cm^2 with a 450 ps pulse duration. The effects of laser fluence, initial ink concentration (10% and 20%), and tattooed dermis thickness (0.05 and 0.07 mm) on temperature and pigment removal efficiency were analyzed. Model validation against numerical and experimental data demonstrated strong agreement. Results indicate that higher fluence significantly enhances pigment removal, whereas greater ink concentration and thicker tattooed dermis increase the required number of sessions. The predicted number of sessions (3–7) aligns well with clinical observations, confirming the model's reliability. The proposed framework establishes a predictive basis for optimizing laser parameters and supports personalized, more efficient tattoo removal treatments.

1. Introduction

Tattoos have gained widespread popularity across various age groups and cultures; however, many individuals later seek their removal for personal, professional, or medical reasons. Among the available techniques, laser treatment has become the gold standard due to its high precision, minimal invasiveness, and ability to selectively target tattoo pigments without causing significant damage to surrounding tissues [1,2]. The efficacy of laser tattoo removal depends on several key parameters, including laser wavelength, fluence, pulse duration, spot size, ink type, pigment depth, and particle size [3]. Optimizing these parameters is essential to maximize pigment clearance while minimizing undesirable side effects such as scarring, hypopigmentation, or incomplete pigment removal [4].

The fundamental mechanism underlying laser tattoo removal is selective photothermolysis, wherein light energy is preferentially absorbed by tattoo pigments exhibiting higher optical absorption coefficients than the surrounding dermis [5]. The wavelength is chosen according to the absorption spectrum of the pigment—for instance, 532 nm for red pigments and 1064 nm for darker pigments such as black or blue [6,7]. Upon absorption, laser energy is rapidly converted into thermal and mechanical effects, resulting in intense localized heating and the generation of shock waves within short pulse durations [8,9]. These effects induce pigment fragmentation through thermal expansion and stress, reaching peak temperatures of approximately 1400 °C, which, if not properly controlled, may risk adjacent tissue damage [10]. The resulting microscopic debris is subsequently cleared through lymphatic drainage and immune processes over the weeks following treatment [10,40].

In clinical practice, the effectiveness of tattoo removal is typically determined empirically based on physician experience, resulting in

* Corresponding author.
E-mail address: Ratphadu@engr.tu.ac.th (P. Rattanadecho).

https://doi.org/10.1016/j.icheatmasstransfer.2026.111192

Available online 10 April 2026

Nomenclature

c	Speed of light in the tissue (m/s)
c_{ink}	Ink concentration (kg/m^3)
C	Specific heat capacity (J/kg K)
D	Optical diffusion coefficient (m)
D_{td}	Tattooed dermis thickness (mm)
g	Anisotropy factor
k	Thermal conductivity (W/m K)
L	Latent heat (kJ/kg)
$m_{ink,d}$	Rate of ink degradation (kg/m^{3s})
n	Refractive index
P_{laser}	Fluence rate (J/cm^2)
Q_{evap}	Heat loss due to water evaporation (W/m^3)
Q_{ext}	External heat source term due to laser irradiation (W/m^3)
Q_{met}	Metabolic heat generation (W/m^3)
R	Ratio of reflected light
T	Temperature (K)
V_{ink}	Volume fraction of ink
$W(T)$	Water tissue density as temperature function (kg/m^3)
$W_{ink}(T)$	Ink density as temperature function (kg/m^3)
t	Time (s)
x	Spatial coordinate or space dimension (m)

Greek symbols

ρ	Density (kg/m^3)
$\varnothing$	Light intensity (W/m^2)
ω_b	Blood perfusion rate (1/s)
μ_a	Absorption coefficient (1/s)
μ_b	Scattering coefficient (1/m)

Subscript

b	blood
ink	ink
met	metabolic
ext	external

considerable variability in treatment outcomes, the number of required sessions, and overall patient satisfaction. To address these inconsistencies, mathematical and computational modeling has been increasingly employed to investigate the underlying mechanisms of laser–tissue and laser–ink interactions. Such models provide a cost-effective and noninvasive framework for analyzing the effects of laser parameters, tissue optical properties, and ink characteristics, thereby complementing experimental and clinical observations.

Over the past decade, modeling approaches in laser therapy have been successfully applied to a wide range of biomedical problems [11–13], including laser hair removal [14], laser skin welding [15,16], and tumor ablation [17,18]. Furthermore, the thermo-mechanical behavior of skin tissue under laser irradiation has been extensively investigated [14,19–21], demonstrating the capability of mathematical models to describe coupled heat transfer, stress evolution, and deformation phenomena in biological tissues exposed to laser energy. However, previous studies on laser tattoo removal have employed both numerical and experimental methods to elucidate the physical processes governing pigment elimination, such as pressure-wave generation and stress distribution [22,23], particle fragmentation [24], and pigment clearance dynamics [25]. These simulations have further enabled direct visualization of the photomechanical mechanism during laser tattoo removal [26,27], providing deeper insight into transient thermo-mechanical responses that are often difficult to capture. Such findings complement theoretical modeling efforts and contribute to a more comprehensive understanding of the underlying mechanisms governing laser tattoo removal. In addition, nevus of Ota treatment is similar to laser tattoo removal in that both involve laser interactions with pigmented lesions in the skin. Accordingly, previous simulation studies on nevus of Ota, such as those by Xiao et al. [41] and Deng et al. [42], are also relevant to the present work. In particular, these studies employed local non-equilibrium heat transfer models to analyze the thermal response during laser treatment, while laser energy deposition and light propagation in tissue were evaluated using the Monte Carlo method. Therefore, these studies provide a relevant theoretical basis for the present work, while the current study extends the analysis specifically to laser tattoo removal.

Although these studies have substantially advanced the understanding of laser–tissue interactions, most have primarily focused on transient thermal and mechanical responses. Moreover, in the context of mathematical modeling, only a few studies have presented comprehensive frameworks capable of analyzing optical parameters and quantitatively predicting the required number of treatment sessions. Hence, the present study developed a one-dimensional Multiphysics model of multilayered skin using COMSOL Multiphysics to simulate coupled laser–tissue interactions during tattoo removal, focusing on the light, thermal, and mass responses such as laser intensity, temperature distribution, and residual ink concentration. The model integrates the light transport, bioheat transfer, and mass transfer equations to describe the coupled mechanisms of heat transfer and ink-mass reduction governing energy absorption and pigment decomposition within the tattooed dermis. The reliability of the model was assessed by validating the simulation results against both numerical and experimental data, as well as available clinical reports. The proposed model provides a quantitative and predictive tool for optimizing laser parameters, minimizing inter-patient variability, and supporting personalized and efficient tattoo-removal planning. This work bridges biomedical laser applications with the fundamental theories, underscoring the importance of Multiphysics coupling in accurately predicting therapeutic outcomes.

2. Methods and model

Fig. 1(a) illustrates the schematic diagram of the laser tattoo removal process. In the simulation, an Nd:YAG laser with a wavelength of 1064 nm was applied at fluence levels of 0.3, 4, and 6 J/cm^2, with a pulse duration of 450 ps. These laser parameters were selected based on published treatment guidelines for the PicoWay laser system in skin of color [39]. The selected fluence values fall within the clinically reported treatment range of the PicoWay system. In addition, the simulated condition corresponds to the 1064-nm picosecond Nd:YAG configuration of the PicoWay platform (Syneron Candela Corp., Wayland, MA, USA), for which a pulse duration of 450 ps has been reported in clinical studies and technical specifications [35,36].

Moreover, Fig. 1(b) presents the one-dimensional computational model developed using COMSOL Multiphysics. The model was designed to simulate coupled light, heat, and mass transfer phenomena within multilayered skin tissue. A one-dimensional geometry was adopted because the skin thickness is relatively small compared with the laser spot size. However, previous studies have also shown that the laser spot diameter affects the penetration depth of pulsed lasers [43], indicating that spot size remains an important factor in laser energy deposition. Since the present model focuses on the local laser–tissue response beneath the irradiated region, and actual laser tattoo removal is typically performed by repetitive scanning over the skin surface, each irradiated location can be reasonably approximated as a local one-dimensional problem in the depth direction. Therefore, the one-dimensional assumption was considered appropriate for the present analysis, while also reducing the computational cost compared with

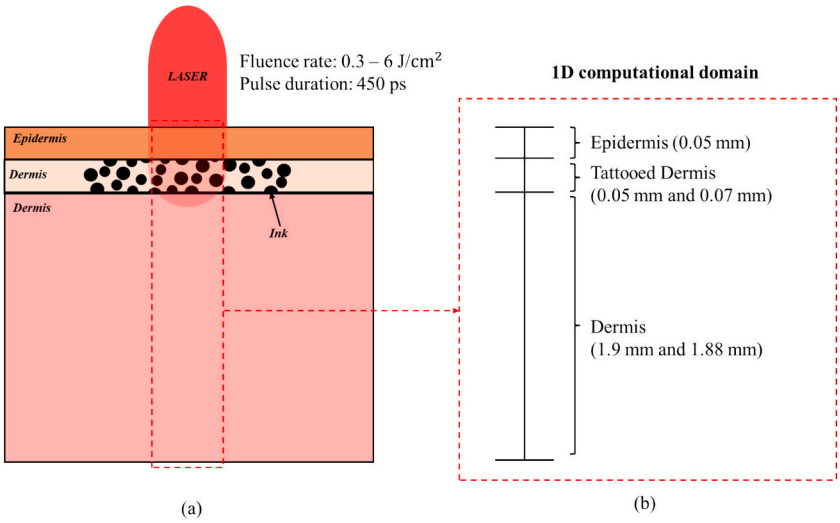

Fig. 1. (a) Schematic diagram of laser tattoo removal treatment and (b) 1D computational domain.

two- or three-dimensional models. The simulations were performed to examine the temperature distribution, ink concentration reduction, and to estimate the number of treatment sessions required for complete tattoo removal.

2.1. Physical model

The computational domain consisted of three layers: the epidermis (0.05 mm), the tattooed dermis (0.05 and 0.07 mm), and the dermis (1.90 and 1.88 mm). Tattoo pigment has been reported to be deposited in skin layers beneath the epidermal tissue [10,28]. Sardana et al. [10] reported an ink deposition depth of approximately 0.4 mm, whereas Izikson et al. [28] provided photographic evidence from porcine skin confirming pigment deposition below the epidermal tissue, although the corresponding depth was not quantitatively specified. Accordingly, the thickness of the tattooed dermis adopted in the present model was assumed. The tattooed dermis was further assumed to contain ink concentrations of 10% and 20% by volume, representing different pigment densities within the tissue. In addition, the pigment particles were assumed to be uniformly distributed and isotropic within the tattooed dermis, corresponding to two initial ink concentration scenarios (V_{ink} = 0.1 and 0.2), as described in the previous section.

2.2. Light transport analysis

Laser energy deposition within the skin layers was described using the diffusion approximation for light transport, which has been widely applied in similar laser–tissue interaction studies [14,21,29,30]. The governing time-dependent diffusion equation employed in the present study was adopted from Patterson et al. [38]. For simplification of the problem, the following assumptions are made:

(1) The skin tissue was assumed to be optically homogeneous and isotropic within each layer.

(2) The optical properties were assumed to be constant.

(3) The effect of ink density variation on optical properties was ignored.

$$\frac{1}{c}\frac{\partial}{\partial t}\varnothing - D\nabla^2\varnothing + \mu_a\varnothing = S \tag{1}$$

$$D = [3(\mu_a + (1-g)\mu_s)]^{-1} \tag{2}$$

Where $\varnothing$ is the intensities of laser (W/m^2), D is the optical diffusion coefficient (m) of skin tissue, c is the speed of light in the human skin (m/s), μ_a is the absorption coefficient (1/m) of skin, μ_s is the scattering coefficient (1/m) and g is the optical anisotropy factor, S is the laser source (W/m^3). At the skin surface (x = 0 mm), the laser is assumed to deliver continuous and uniform irradiation in the depth direction. A Gaussian beam profile was not considered, since the present one-dimensional model represents the central region of the laser beam and simplifies the light transport analysis.

$$-\boldsymbol{n}\bullet(-D\nabla\varnothing) = (1-R)P(t)_{laser} \tag{3}$$

Where $P(t)_{laser}$ is the laser irradiance at the upper surface (W/m^2). The lower surface $(x = 2\,mm)$ is assumed that laser flux continuous boundary condition.

$$-\boldsymbol{n}\bullet(-D\nabla\varnothing) = 0 \tag{4}$$

The internal interfaces between each tissue are assumed to be under continuity boundary condition.

$$\boldsymbol{n}\bullet(D\nabla\varnothing_u - D\nabla\varnothing_d) = 0 \tag{5}$$

2.3. Heat transfer analysis

The temperature evolution within each layer was analyzed using a modified Pennes bioheat equation that incorporated laser energy deposition and water evaporation [31,32]. The following assumptions were made:

(1) The skin tissue properties were assumed to be isotropic and homogeneous.

(2) Thermal properties such as tissue density, specific heat capacity, thermal conductivity, and blood perfusion rate were considered constant.

(3) The effect of ink density variation on thermal properties was neglected.

(4) The interfaces between the tissue layers were assumed to be smooth.

(5) Water evaporation was considered according to the water tissue density function.

(6) Laser energy was included as an external heat source term.

$$\rho C\frac{\partial T}{\partial t} = \nabla\bullet(k\nabla T) + \rho_b C_b\omega_b(T_b - T) + Q_{met} + Q_{laser} + Q_{evap} \tag{6}$$

$$Q_{laser} = \mu_a\varnothing \tag{7}$$

$$Q_{evap} = m_{evap}L \tag{8}$$

Where ρ is tissue density (kg /m^3), C is tissue heat capacity (J/kg K),

k is thermal conductivity (W/m K), T_b is the blood temperature (37°C), ρ_b is the blood density (1060 kg/m^3) [20], C_b is the specific heat capacity of the blood (3660 J/kg K) [20], ω_b is the rate of blood perfusion (1/s), Q_{met} is metabolic heat generation (W/m^3), Q_{laser} considering of term external heat sources of laser deposition (W/m^3), and Q_{evap} is the heat loss due to water evaporation (W/m^3), L is latent heat (2260 kJ/kg) [32]. Yang et al. [32] introduced the water content as the function of temperature during thermal ablation process. Hence, the water change due to water evaporation is described as functions of temperature as follows:

$$W(T) = 778 \times \begin{cases} 1 - \exp\left(\dfrac{T-106}{3.42}\right) & T \le 103 \\ 0.03713T^3 + 11.47T^2 + 1182T - 40582, & 103 < T \le 104 \\ \exp\left(\dfrac{80-T}{34.37}\right) & T > 104 \end{cases} \tag{9}$$

According to the present three-layer model, consisting of the epidermis, dermis, and tattooed dermis, the water content function proposed by Yang et al. [32] has been modified. The modified expression is given as follows:

$$W(T) = W_i\rho_i \times \begin{cases} 1 - \exp\left(\dfrac{T-106}{3.42}\right) & T \le 103 \\ 0.03713T^3 + 11.47T^2 + 1182T - 40582, & 103 < T \le 104 \\ \exp\left(\dfrac{80-T}{34.37}\right) & T > 104 \end{cases} \tag{10}$$

The water evaporation rate was calculated using the chain rule derivative of $W(T)$ as follows:

$$m_{evap} = \frac{dW(T)}{dt} = \frac{\partial W(T)}{\partial T}\frac{\partial T}{\partial t} \tag{11}$$

Where W_i is initial water contents of each layer (%), which assume to be 70% for all layers. In addition, the thermal conductivity of the skin tissue, influenced by the presence of tattoo ink within the tattooed dermis, is determined using Eq. (12) [34].

$$\frac{1}{k_{mix}} = \frac{1 - V_{ink}}{k_{dermis}} + \frac{V_{ink}}{k_{\text{tattoo}}} \tag{12}$$

where k_{mix} is the effective thermal conductivity of the tattooed dermis (W/m K), V_{ink} is the volume fraction of tattoo ink, k_{dermis} is the thermal conductivity of dermis, and k_{tattoo} is the thermal conductivity of the tattoo ink. For boundary conditions, the skin surface ($x = 0\ mm$) under convection boundary conditions.

$$-\boldsymbol{n} \bullet (k\nabla T) = h_T(T_{air} - T) \tag{13}$$

Where T_{air} is the ambient temperature (25°C) and h_T is heat transfer coefficient (10 W/(m^2 K). The internal interfaces between each tissue are smooth, which means no contact thermal resistance. So, it is assumed to be under a continuity boundary condition.

$$\boldsymbol{n} \bullet (k_u\nabla T_u - k_d\nabla T_d) = 0 \tag{14}$$

2.4. Ink concentration analysis

The temporal variation of ink concentration in the tattooed dermis was modeled using the species equation. The following assumptions were made:

(1) Ink particles were uniformly distributed within the tattooed dermis at the initial state.

(2) Ink diffusion within the tissue was neglected to simplify the analysis of laser-induced pigment fragmentation, as pigment mobility is extremely low in skin tissue.

(3) Ink degradation was governed by a reaction rate dependent on local temperature.

(4) Mass exchange between adjacent layers was neglected.

$$\frac{\partial c_{ink}}{\partial t} = m_{ink,d} \tag{15}$$

The rate of ink degradation was calculated using the chain rule derivative of ink density, $W_{ink}(T)$ as follows:

$$m_{ink,d} \begin{cases} \dfrac{dW_{ink}(T)}{dt}, & c_{ink} > 0 \text{ kg}\Big/\text{m}^3 \\ 0, & c_{ink} \le 0 \text{ kg/m} \end{cases} \tag{16}$$

Where

$$\frac{dW_{ink}(T)}{dt} = \frac{W_{ink}(T)}{\partial T}\frac{\partial T}{\partial t} \tag{17}$$

c_{ink} is ink concentration (kg/m^3), $m_{ink,d}$ is the rate of ink degradation (kg/m^3 s), $W_{ink}(T)$ is the temperature-dependent density (kg/m^3) [24] is shown in Fig. 2. In addition, the piecewise function in Eq. (16) ensures that ink degradation occurs only in local regions where ink still exists ($c_{ink} > 0$). Once the pigment is fully decomposed ($c_{ink} \le 0$), the degradation rate becomes zero. This mechanism reflects the physical reality of laser tattoo removal, preventing non-physical negative concentrations. For the boundary conditions, the upper ($x = 0.05\ mm$) and bottom tattooed dermis layer are under no flux boundary conditions as follows:

$$-\boldsymbol{n} \bullet (D_{ink}\nabla c_{ink}) = 0 \tag{18}$$

For the initial condition, the initial temperature was set to 37 °C, the initial intensity was 0 W/m^2, and initial ink concentration (V_{ink}) was set to 10% and 20% of tattoo density.

3. Numerical procedure

The computational model was implemented in COMSOL Multiphysics using a one-dimensional geometry to represent multilayered skin consisting of the epidermis, tattooed dermis, and dermis. The heat transfer analysis was performed using the Heat Transfer in Solids module, while the light transport and ink degradation analyses were implemented through the coefficient form PDE interfaces. A time-dependent study was conducted to simulate a single laser pulse with a duration of 450 ps at a wavelength of 1064 nm and fluence levels of 0.3, 4, and 6 J/cm^2. All material properties used in the present study are listed in Table 1. A non-uniform mesh was employed based on the mesh

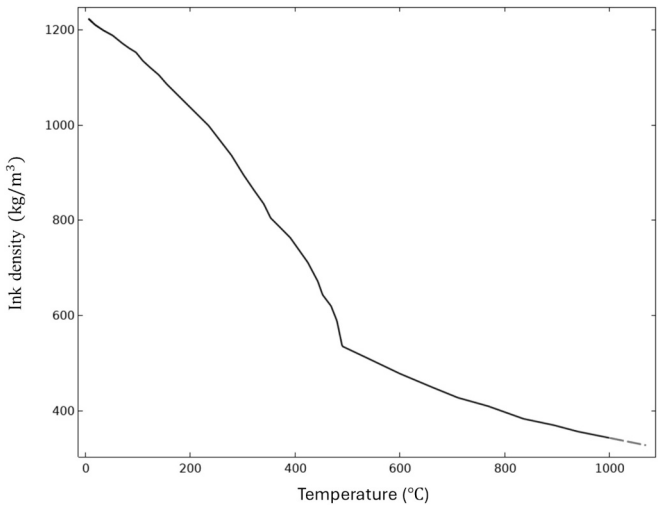

Fig. 2. Temperature-dependent ink density used in ink degradation modeling. [24].

Table 1
Thermal, mechanical and optical properties used in this study.

Properties	Epidermis	Dermis	Ink tattoo	Tattooed dermis ($V_{ink} = 0.1$)	Tattooed dermis ($V_{ink} = 0.2$)
Density, ρ (kg/m^3)	1200 [14]	1090 [14]	1220 [24]	1103	1116
Specific heat of tissue, C (J/Kg K)	3950 [14]	3350 [14]	1800 [24]	3179	3011
Thermal conductivity, k (W/m K)	0.24 [14]	0.42 [14]	46.19 [24]	0.47	0.52
Blood perfusion, ω_b (1/s)	–	0.0031 [20]	–	0.0031 [20]	0.0031 [20]
Metabolic heat generation, Q_{met}(W/m^3)	–	368 [20]	–	368 [20]	368 [20]
Absorption coefficient, μ_a (1/m), 1064 nm	571.16 [33]	25.24 [33]	525,300 [23]	52,553	105,080
Scattering coefficient, μ_s (1/m), 1064 nm	19,073 [33]	11,383 [33]	11,500 [23]	11,395	11,407
Anisotropy, g, 1064 nm	0.85 [22]	0.85 [22]	0.85 [22]	0.85 [22]	0.85 [22]
Refractive index, n	1.37 [29]				
Ratio of reflected light, 1064 nm	0.05 [13]				

convergence analysis, as shown in Fig. 4. Specifically, local mesh refinement was applied in the epidermis and tattooed dermis, with an element size of 5×10^{-6} mm, while a coarser mesh with an element size of 2×10^{-2} mm was used in the dermis. The total number of elements in the computational domain was approximately 20,000. To enhance computational stability, the physics interfaces for light transport, heat transfer, and ink concentration were solved sequentially using a segregated solver. The maximum number of nonlinear iterations per segregated step was set to 20. Adaptive time stepping with a relative tolerance of 1×10^{-4} was employed, and the initial and maximum time steps were set to 0.001 and 1 ps, respectively. The key simulation outputs included temperature distribution, maximum temperature, ink concentration reduction, and the estimated number of treatment sessions.

4. Validation of the model

The experimental and numerical results reported by Paul and Paul [34] were used to evaluate the accuracy of the present numerical model under identical testing conditions. In their experiment, an agar-based tissue phantom was irradiated using a continuous-wave laser with a wavelength of 800 nm. The incident laser power was assumed to follow a Gaussian distribution [17,30], with an average beam intensity of 32,000 W/m^2 and a beam radius of 2.5 mm. The optical and physical properties of the tissue phantom used in the simulation are summarized in Table 2, based on data obtained from the literature [34]. In addition, numerical results from Preechaphonkul et al. [21] were employed to further validate the accuracy of the proposed model under similar simulation conditions. The light intensity distribution at a wavelength of 500 nm was selected for comparison.

5. Results and discussion

5.1. Validation of simulation results

The validity of the present model was evaluated by comparing the predicted temperature evolution in a tissue phantom with existing experimental data. The simulation results showed close agreement with the experimental measurements reported by Paul and Paul [34], as presented in Fig. 3(b), confirming that the model accurately reproduces the thermal response under laser irradiation. Furthermore, the light intensity distribution obtained from the light transport model in the present study exhibited strong consistency with the numerical results of Preechaphonkul et al. [21], as illustrated in Fig. 3(c). These validations confirm the reliability of the proposed numerical framework for tattoo removal simulations.

Table 2
Properties of tissue phantom [34].

Properties	Phantom Tissue (agar)
Tissue density,ρ (kg/m^3)	1050
Specific heat of tissue, C (J/(Kg K))	4219
Thermal conductivity, k (W/(m K))	0.66
Absorption coefficient, μ_a (1/m)	530
Scattering coefficient, μ_s (1/m)	40

5.2. The light transport though skin

Fig. 5 presents the spatial distribution of laser intensity across the skin layers for fluences of 0.3, 4, and 6 J/cm^2, with ink volume fractions (V_{ink}) of 0.1 and 0.2. In all cases, the laser intensity decreases gradually within the epidermis and drops sharply upon entering the tattooed dermis. This discontinuity at the epidermis–tattooed dermis interface results from the pronounced difference in optical absorption and scattering between pigmented and non-pigmented tissues, corresponding to the variation in the optical diffusion coefficient of each layer, as summarized in Fig. 6. This behavior demonstrates the limited light penetration in regions with significantly different optical properties, such as the epidermis, dermis, and tattooed dermis. Moreover, the initial ink concentration strongly influences light transport. At lower ink concentrations ($V_{ink} = 0.1$), the laser penetrates more deeply into the tattooed dermis, whereas higher ink concentrations ($V_{ink} = 0.2$) lead to stronger attenuation and shallower penetration. This trend is consistent across all fluence levels considered (0.3, 4, and 6 J/cm^2) and has practical implications for the treatment of pigments located deeper within the dermis. These results highlight that both laser fluence and ink concentration play a critical role in determining energy deposition and penetration depth.

5.3. The temperature distribution

Figs. 7 and 8 present the temperature distributions across the skin layers for fluences of 0.3, 4, and 6 J/cm^2, with ink volume fractions (V_{ink}) of 0.1 and 0.2. In all cases, a sharp temperature peak is observed at the beginning of the tattooed dermis layer (x = 0.05 mm), corresponding to the region of maximum optical absorption due to the high pigment concentration. This localized heating arises from the higher absorption coefficient of the tattooed dermis compared to other layers. Increasing the laser fluence from 0.3 to 6 J/cm^2 markedly elevates the peak temperature. The maximum temperatures under all conditions are summarized in Fig. 9, which reveals that higher initial ink concentrations lead to greater peak temperatures, reflecting enhanced optical absorption. For a tattooed dermis thickness of 0.05 mm, the maximum temperatures are 97.1 °C ($V_{ink} = 0.1$) and 101.2 °C ($V_{ink} = 0.2$) at 0.3 J/cm^2; 875.2 °C ($V_{ink} = 0.1$) and 2188.4 °C ($V_{ink} = 0.2$) at 4 J/cm^2; and 1516.9 °C ($V_{ink} = 0.1$) and 3499.8 °C ($V_{ink} = 0.2$) at 6 J/cm^2. A similar trend is observed for the 0.07 mm tattooed dermis The high temperature predicted in Figs. 7 and 8 is consistent with previous simulation findings. Humphries et al. [23] also reported markedly elevated temperatures under laser irradiation, in the range of approximately 200–4300 °C, with the temperature strongly dependent on the applied fluence. A similar trend was observed in the present study, where the temperature decreased across the tattooed dermis with increasing distance from the

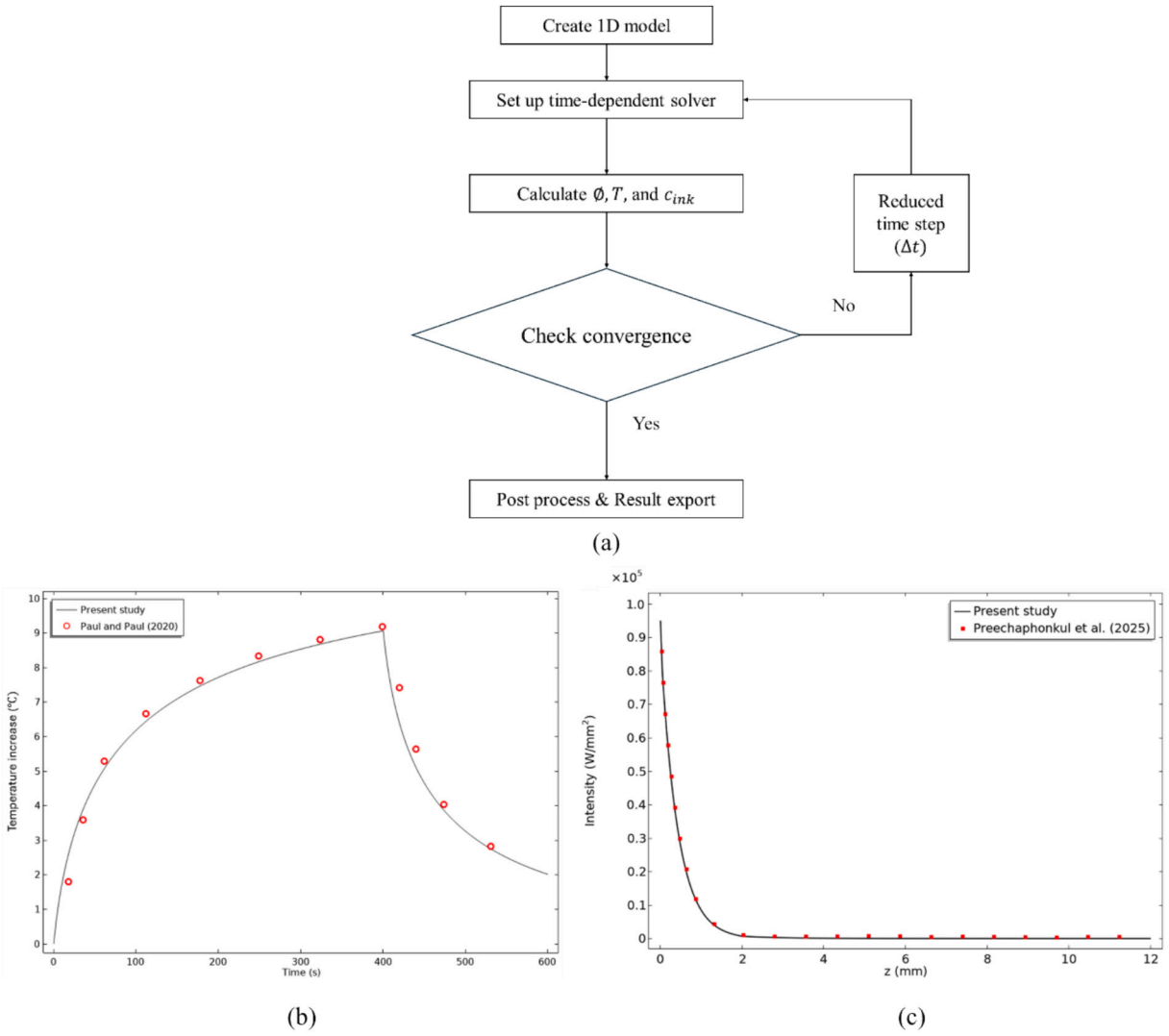

Fig. 3. (a) The computational workflow, and (b) comparison of temperature rise between the present study and experimental data from Paul and Paul [34] and (c) comparison of intensity between the present study and numerical result obtained Preechaphonkul et al. [21].

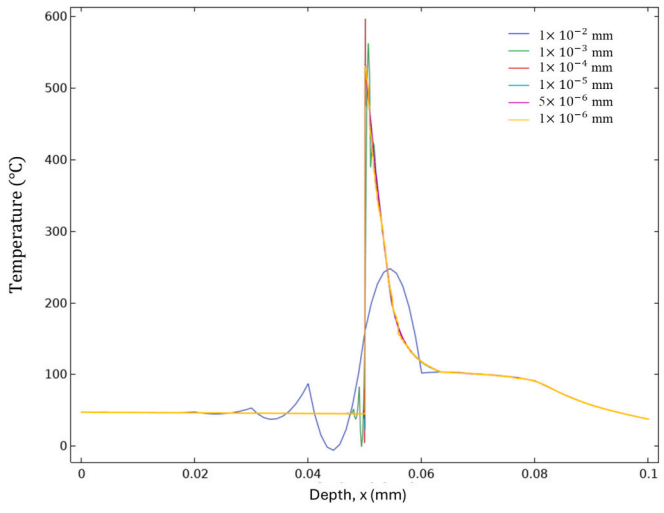

Fig. 4. Effect of mesh size on a spatial temperature profile across skin layers.

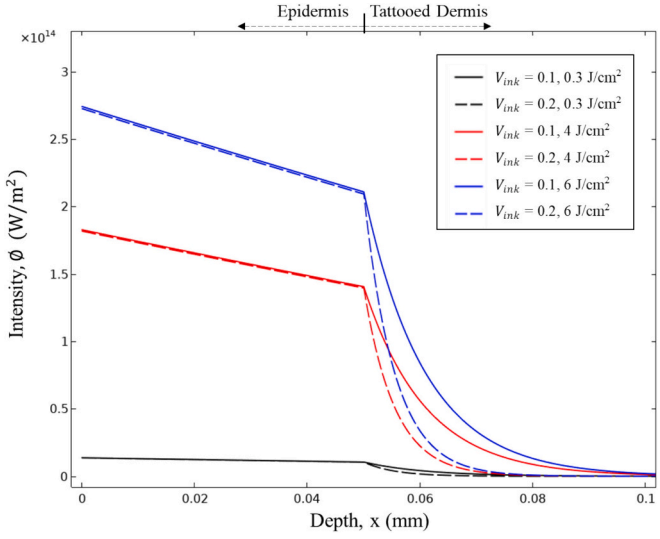

Fig. 5. The spatial distribution of laser intensity within the skin layers for fluences of 0.3, 4, and 6 J/cm^2 and ink volume fractions of 0.1 and 0.2.

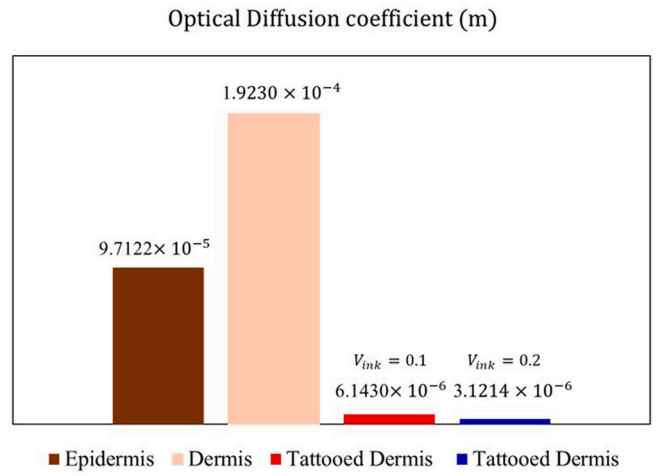

Fig. 6. Optical diffusion coefficients of epidermis, dermis, and tattooed dermis.

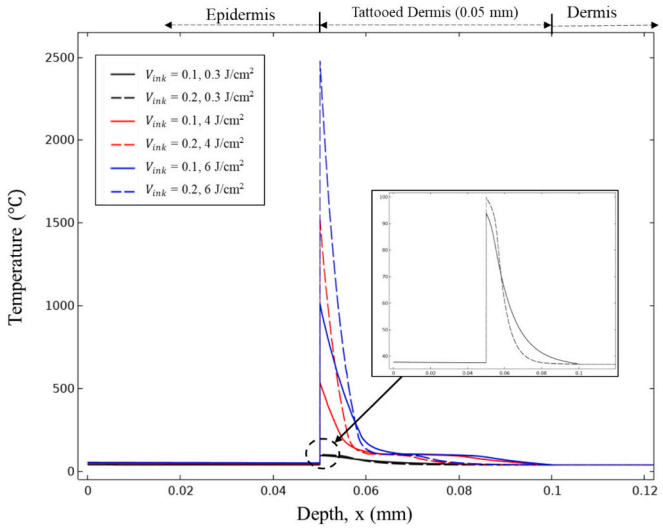

Fig. 7. Temperature distribution along the skin depth under different laser fluences and ink volume fractions for tattooed dermis of 0.05 mm.

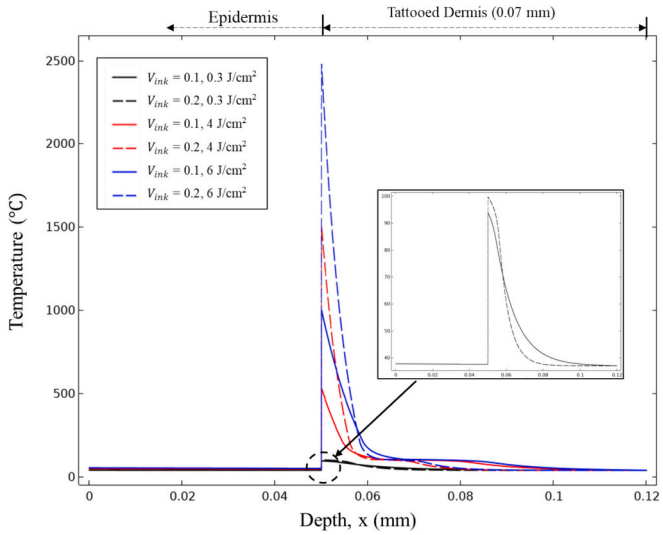

Fig. 8. Temperature distribution along the skin depth under different laser fluences and ink volume fractions for tattooed dermis of 0.07 mm.

heat source. This further supports that the maximum temperature is highly localized and occurs only within a limited region during laser irradiation. The elevated temperature in the present study occurs only momentarily during laser irradiation and represents a highly transient local response after the pigment absorbs laser energy. Such a rapid and intense temperature rise may be sufficient to induce plasma-related phenomena, which have been suggested to contribute to pigment fragmentation and redistribution during tattoo removal [23,26]. Therefore, the predicted high temperature in the present study is physically plausible under localized laser–pigment interaction conditions. These results demonstrate the significant influence of laser fluence on the thermal response during tattoo removal. Increasing the laser fluence leads to a pronounced temperature rise, particularly within ink-pigment-rich regions such as the tattooed dermis. Moreover, the lower temperature regime at 0.3 J/cm^2 appears insufficient for pigment fragmentation. The steep temperature gradient at the tattooed dermis interface further indicates limited thermal diffusion during the 450 ps pulse, thereby minimizing collateral thermal damage to adjacent tissues. The simulations highlight the critical interplay between laser fluence and ink concentration in determining the efficiency and safety of the tattoo removal process. While high fluence levels generate the intense localized heating necessary for effective pigment fragmentation, excessive energy delivery may induce overheating and potential damage to thermally sensitive skin structures.

5.4. The ink concentration

Fig. 10(a) and 10(b) illustrate the spatial distribution of residual ink concentration within the tattooed dermis for two layer thicknesses (0.05 mm and 0.07 mm) under laser fluences of 0.3, 4, and 6 J/cm^2, with ink volume fractions (V_{ink} = 0.1 and 0.2). In all cases, the ink concentration remains nearly constant in regions beyond the primary absorption zone, while a sharp decrease occurs near the surface of the tattooed dermis, corresponding to the region of maximum optical absorption and highest temperature rise. These results indicate that pigment removal occurs in regions where laser energy deposition is highest and the temperature is sufficiently elevated to induce pigment fragmentation. At higher fluences of 4 and 6 J/cm^2, the steep decline in ink concentration near the surface becomes more pronounced compared with 0.3 J/cm^2, indicating enhanced pigment decomposition. The initial ink concentration also influences the reduction pattern: higher concentrations (V_{ink} = 0.2) result in more localized and abrupt decreases near the absorption peak due to concentrated heat absorption, whereas lower concentrations (V_{ink}= 0.1) allow deeper light penetration and lead to a broader, more distributed reduction profile. When comparing the two dermal thicknesses, the thicker tattooed layer (0.07 mm) exhibits a localized degradation pattern concentrated near the upper interface, suggesting that the effective depth of photothermal interaction is confined to the region of highest absorption. Overall, these results demonstrate that the efficiency of laser tattoo removal is governed primarily by laser fluence and initial ink concentration. An optimal combination of high fluence and moderate-to-low pigment concentration enhances localized pigment removal.

5.5. The estimation of laser tattoo removal session

In this section, the estimation of the number of laser tattoo removal treatment sessions was approximated using the simulation results derived from the ink concentration profiles. The percentage of ink removal per session was evaluated using Eq. (19), as expressed below:

$$\text{The ink removal } (\%) = 100 \times \int \frac{(c_{0,ink} - c_{ink})}{c_{0,ink} D_{td}} dx \tag{19}$$

Where D_{td} is the thickness of tattooed dermis (0.05 and 0.07 mm), c_{ink} is current ink concentration (kg/m^3), and $c_{0,ink}$ is the initial

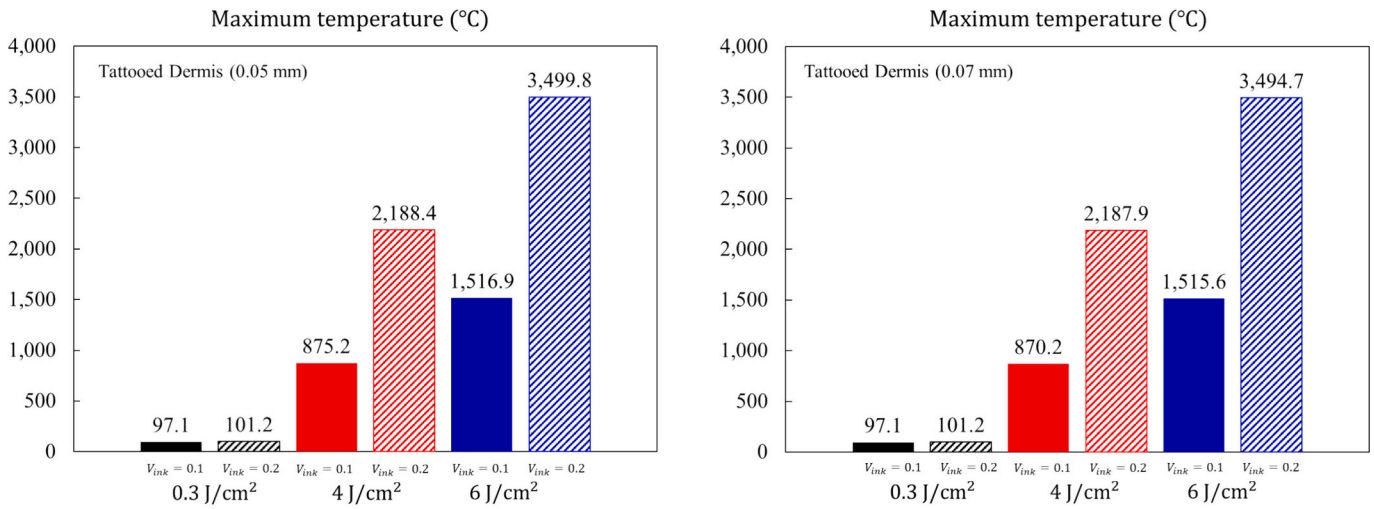

Fig. 9. Maximum tissue temperature across different fluence levels and ink volume fraction.

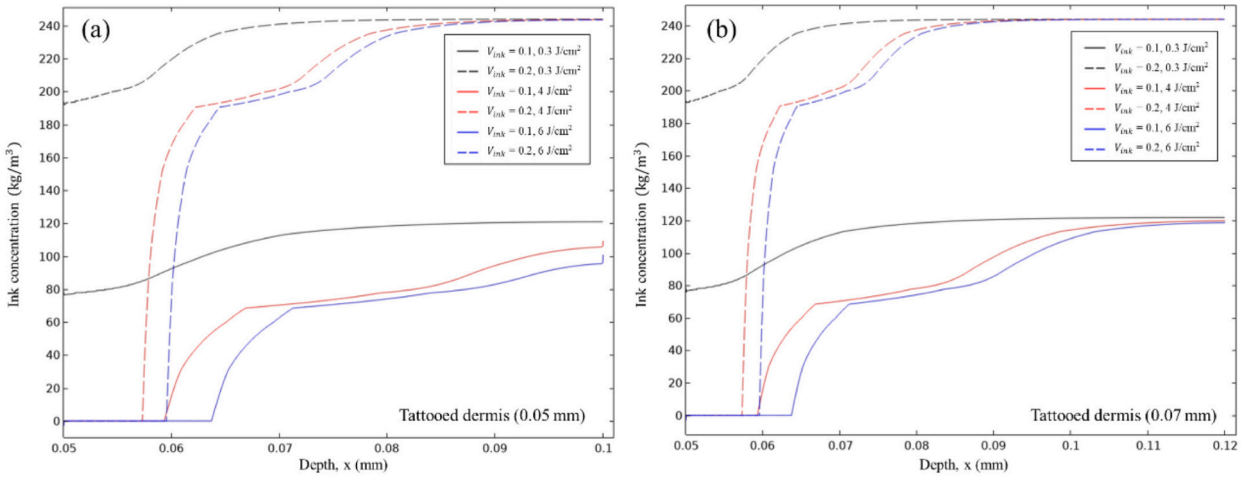

Fig. 10. Ink removal depth per session of various laser fluence for different tattooed dermis thickness and ink concentrations.

Table 3
Reports obtained from literature of laser tattoo removal by picosecond laser tattoo removal treatment.

Author	Wavelength	Energy setting (J/cm²)	Pulse duration (ps)	No. sessions	Ink type
Lorgeou et al. [35]	1064	2–8.4	450	2 – 4	Black
Bernstien et al. [36]	1064	0.65	450	7	Black
Ross et al. [37]	1064	0.4	35	4	Black, Blue, Green, Purple

concentration (kg/m³).

The clinical data reported in the literature were summarized in Table 3 and serve as benchmark references to assess the reliability of the present model. The simulated percentage of ink removal per session and the estimated number of treatment sessions are presented in Table 4. For all cases, the results confirm that the laser parameters strongly influence treatment outcomes. High-fluence irradiation (4–6 J/cm²) provides more efficient tattoo removal compared to low fluence (0.3 J/cm²), as the latter requires a greater number of treatment sessions (12–28 sessions) to achieve comparable ink clearance. In addition, a higher initial

Table 4
Estimated number of treatment sessions required for laser tattoo removal based on laser fluence levels and different tattooed layer thickness.

Fluence (J/cm²)	V_{ink} (–)	Pulse width (ps)	Tattooed dermis thickness, D (mm)	Ink removed per session (%),*Removed*%	Estimated Session $N = \frac{100}{Removed\%}$
0.3	0.1	450	0.05	8.51	11.75 ≈12
0.3	0.2	450	0.05	3.67	27.24 ≈28
4	0.1	450	0.05	39.49	2.53 ≈3
4	0.2	450	0.05	20.31	4.92 ≈5
6	0.1	450	0.05	47.36	2.11 ≈2
6	0.2	450	0.05	24.70	4.05 ≈ 5
0.3	0.1	450	0.07	6.17	16.21 ≈17
0.3	0.2	450	0.07	2.62	38.13 ≈39
4	0.1	450	0.07	29.41	3.40 ≈4
4	0.2	450	0.07	14.49	6.90 ≈ 7
6	0.1	450	0.07	35.57	2.81 ≈ 3
6	0.2	450	0.07	17.65	5.66 ≈ 6
0.65	0.1	450	0.05	14.65	6.82 ≈ 7
0.65	0.2	450	0.05	5.46	18.30 ≈ 19
0.4	0.1	35	0.05	10.59	9.44 ≈10
0.4	0.2	35	0.05	4.27	23.39 ≈ 24

ink concentration (V_{ink} = 0.2) slightly reduces the percentage of ink removed per session; consequently, more sessions are required compared to lower ink concentrations (V_{ink}= 0.1).

Furthermore, the thickness of the tattooed dermis also influences the treatment outcome. Thicker layers require more sessions due to deeper pigment distribution and reduced light penetration, which result in a larger amount of residual ink pigment initially retained within the skin tissue. It should be noted that the thickness of the tattooed dermis represents the degree of pigment deposition, where a thicker layer typically indicates a denser and more concentrated ink distribution. The estimated number of sessions (N) ranges from 3 to 5 sessions for fluences of 4–6 J/cm^2 with a tattooed dermis thickness of 0.05 mm, showing strong agreement with clinical observations reported by Lorgeou et al. [35], who documented 2–4 sessions under comparable conditions. At a fluence of 0.65 J/cm^2 and a dermis thickness of 0.05 mm, the model predicts approximately 7 sessions, which matches the 7 sessions reported by Bernstein et al. [36]. In contrast, the model slightly overpredicts the required number of sessions, estimating 10 sessions compared with 4 sessions reported by Ross et al. [37] at a fluence of 0.4 J/cm^2. However, it should be noted that the present model does not explicitly account for microbubble or cavitation effects around heated pigment particles. Previous studies have shown that rapid laser heating can induce cavitation bubble formation in the surrounding tissue, which may affect local thermal diffusion, tissue response, and pigment fragmentation behavior [26,27,44]. In addition, cavitation bubble expansion may generate local mechanical stress and contribute to tissue damage near the pigment particles [22]. Therefore, the present model should be interpreted as a simplified representation focused on light transport, heat transfer, and mass transport, while bubble-related effects remain a limitation to be addressed in future studies. Consequently, the proposed model showed good predictive performance by capturing the relationship between fluence, pigment characteristics, and treatment efficiency. These findings support the capability of the model to estimate the required number of treatment sessions and to identify suitable fluence ranges for different clinical scenarios, thereby providing a useful computational framework for treatment planning and optimization in laser tattoo removal.

6. Conclusion

This study presents a comprehensive Multiphysics model for simulating laser tattoo removal, focusing on the coupled effects of laser fluence, initial ink concentration, and tattooed dermis thickness on treatment efficiency. The model integrates light transport, heat transfer, and mass diffusion phenomena to accurately describe the photothermal response and pigment-removal dynamics within tattooed skin under laser irradiation. Model validation against both experimental data (Paul and Paul [34]) and numerical results (Preechaphonkul et al. [21]) at a wavelength of 500 nm confirms its accuracy and reliability in predicting temperature rise, ink reduction, and spatial energy absorption.

The principal findings are summarized as follows:

(1) Higher fluence levels (4–6 J/cm^2) yield significantly greater tattoo-removal efficiency compared with 0.3 J/cm^2, due to enhanced pigment fragmentation and increased optical energy absorption within the tattooed dermis.

(2) The initial ink concentration strongly influences treatment performance; higher pigment densities require a greater number of sessions to achieve complete clearance.

(3) Increasing tattooed-dermis thickness proportionally raises the number of sessions needed for complete removal, owing to deeper pigment embedding and reduced light penetration, which limit the effective energy reaching the deeper pigment regions.

(4) The predicted number of sessions (3–7) shows strong agreement with clinical observations reported by Lorgeou et al. [35], Bernstein et al. [36], validating the model's predictive capability.

The present modeling framework provides an effective computational tool for personalized treatment planning, enabling clinicians to select optimal laser parameters, minimize the number of treatment sessions, and improve both treatment safety and patient satisfaction. Despite its strong predictive capability, several limitations should be acknowledged. The model assumes homogeneous optical and thermal properties across all skin layers, which may not fully capture the inherent heterogeneity of biological tissue. Moreover, the pigment distribution was considered uniform, while in reality, particle size, density, and spatial distribution vary, affecting local light absorption and heat transfer. In addition, the present model could inspire future studies on other thermal therapy modeling applications, particularly those involving complex coupled phenomena.

Future work should focus on extending the model to incorporate multi-wavelength laser simulations for more accurate representation of multicolored tattoos and on including patient-specific parameters—such as pigment type, particle size distribution, and dermal geometry—to enhance clinical realism and predictive accuracy. Such developments will further advance personalized and efficient planning for laser tattoo removal.

CRediT authorship contribution statement

Vannakorn Mongkol: Writing – review & editing, Writing – original draft, Validation, Software, Methodology, Investigation, Formal analysis, Data curation. **Wutipong Preechaphonkul:** Writing – review & editing. **Suphak Khumsupha:** Software, Resources. **Kittipong Junsook:** Validation, Software. **Phadungsak Rattanadecho:** Supervision, Project administration, Funding acquisition.

Declaration of competing interest

The authors declare the following financial interests/personal relationships which may be considered as potential competing interests:

Phadungsak Rattanadecho reports financial support was provided by National Research Council of Thailand. Vannakorn Mongkol reports financial support was provided by National Research Council of Thailand. If there are other authors, they declare that they have no known competing financial interests or personal relationships that could have appeared to influence the work reported in this paper.

Acknowledgement

This research project is supported by National Research Council of Thailand (NRCT): (Contact No. N41A640213), Thailand Science Research (TSRI) Fundamental Fund, fiscal year 2025, and Thailand Science Research (TSRI) Fundamental Fund, fiscal year 2026.

Data availability

No data was used for the research described in the article.

References

[1] I. Kurniadi, F. Tabri, A. Madjid, A.I. Anwar, W. Widita, Laser tattoo removal: fundamental principles and practical approach, Dermatol. Ther. 34 (2021) e14418, https://doi.org/10.1111/dth.14418.
[2] R. Small, A Practical Guide to Laser Procedures, Lippincott Williams & Wilkins, 2015.
[3] L. Hernandez, N. Mohsin, F.S. Frech, I. Dreyfuss, A. Vander Does, K. Nouri, Laser tattoo removal: laser principles and an updated guide for clinicians, Lasers Med. Sci. 37 (2022) 2581–2587, https://doi.org/10.1007/s10103-022-03576-2.
[4] L.I. Naga, T.S. Alster, Laser tattoo removal: An update, Am. J. Clin. Dermatol. 18 (2017) 59–65, https://doi.org/10.1007/s40257-016-0227-z.
[5] R.R. Anderson, J.A. Parrish, Selective photothermolysis: precise microsurgery by selective absorption of pulsed radiation, Science 220 (1983) 524–527, https://doi.org/10.1126/science.6836297.
[6] S. Barua, Laser-tissue interaction in tattoo removal by q-switched lasers, J Cutan Aesthet Surg 8 (2015) 5–8, https://doi.org/10.4103/0974-2077.155063.

[7] A.H. Clauer, J.H. Holbrook, B.P. Fairand, Effects of laser induced shock waves on metals, in: Shock Waves and High-Strain-Rate Phenomena in Metals: Concepts and Applications, 1981, pp. 675–702, https://doi.org/10.1007/978-1-4613-3219-0_38.
[8] S. Choudhary, M.L. Elsaie, A. Leiva, K. Nouri, Lasers for tattoo removal: a review, Lasers Med. Sci. 25 (2010) 619–627, https://doi.org/10.1007/s10103-010-0800-2.
[9] C.N. Lee, E.Y. Bae, J.G. Park, S.H. Lim, Permanent makeup removal using q-switched nd: YAG laser, Clin. Exp. Dermatol. 34 (2009) e594–e596, https://doi.org/10.1111/j.1365-2230.2009.03268.x.
[10] K. Sardana, R. Ranjan, S. Ghunawat, Optimising laser tattoo removal, J Cutan Aesthet Surg 8 (2015) 16–24, https://doi.org/10.4103/0974-2077.155068.
[11] M. Azhdari, G. Rezazadeh, L. Lambers, T. Ricken, H.M. Tautenhahn, F. Tautenhahn, S.M. Seyedpour, Refining thermal therapy: temperature distribution modeling with distinct absorption in multi-layered skin tissue during infrared laser exposure, Int. Commun. Heat Mass Transf. 157 (2024) 107818, https://doi.org/10.1016/j.icheatmasstransfer.2024.107818.
[12] M. Azhdari, G. Rezazadeh, T. Ricken, R. Pathak, H.M. Tautenhahn, F. Tautenhahn, S.M. Seyedpour, Temperature distribution in multi-layered skin tissue during laser irradiation considering epidermis sublayers: virtual element method approach, Therm. Sci. Eng. Prog. 59 (2025) 103297, https://doi.org/10.1016/j.tsep.2025.103297.
[13] W. Preechaphonkul, V. Mongkol, P. Promoppatum, V. Srimaneepong, Comparative analysis of repetitive pulsed and continuous laser heating in multi-layered skin: bioheat vs. dual-phase lag model perspective, Int. J. Thermofluids 29 (2025) 101371, https://doi.org/10.1016/j.ijft.2025.101371.
[14] V. Mongkol, W. Preechaphonkul, P. Rattanadecho, Photo-thermo-mechanical model for laser hair removal simulation using multiphysics coupling of light transport, heat transfer, and mechanical deformation (case study), Case Stud. Therm. Eng. 41 (2023) 102562, https://doi.org/10.1016/j.csite.2022.102562.
[15] T. Chabuanoi, N. Pannucharoenwong, P. Wongsangnoi, P. Rattanadecho, J. Saemathong, S. Hemathulin, Simulation effect of laser moving speed and spot size on maximum temperature in laser welding human skin tissue, Eng. Sci. 31 (2024) 1193, https://doi.org/10.30919/es1193.
[16] T. Chabuanoi, N. Pannucharoenwong, P. Wongsangnoi, S. Echaroj, P. Rattanadecho, J. Saemathong, S. Panvichien, Effect of temperature during laser welding of tissue between bioheat model and porous media model by varying 3 pattern of laser movement: single-line, line and zigzag, Eng. Sci. 33 (2024) 1335, https://doi.org/10.30919/es1335.
[17] P. Boontatao, N. Pannucharoenwong, T. Chabuanoi, P. Rattanadecho, T. Tubtawee, S. Panvichien, Simulation of thermal effects on rectal wall during laser treatment of prostate cancer using hyaluronic acid and polyethylene glycol spacers: a generalized dual-phase-lag bioheat approach, Eng. Sci. 33 (2024) 1308, https://doi.org/10.30919/es1308.
[18] P. Boontatao, N. Pannucharoenwong, P. Sermlao, S. Panvichien, Generalized dual-phase-lag modeling of rectal wall thermal protection in prostate laser therapy using hyaluronic acid, collagen, and balloon spacers, Int. J. Heat Mass Transf. 253 (2025) 127570, https://doi.org/10.1016/j.ijheatmasstransfer.2025.127570.
[19] S.M. Seyedpour, M. Azhdari, L. Lambers, T. Ricken, G. Rezazadeh, One-dimensional thermomechanical bio-heating analysis of viscoelastic tissue to laser radiation shapes, Int. J. Heat Mass Transf. 218 (2024) 124747, https://doi.org/10.1016/j.ijheatmasstransfer.2023.124747.
[20] P. Wongchadakul, P. Rattanadecho, T. Wessapan, Implementation of a thermomechanical model to simulate laser heating in shrinkage tissue (effects of wavelength, laser irradiation intensity, and irradiation beam area), Int. J. Therm. Sci. 134 (2018) 321–336, https://doi.org/10.1016/j.ijthermalsci.2018.08.008.
[21] W. Preechaphonkul, V. Mongkol, K. Torsuwan, R. Ungpakorn, T. Hanawa, P. Promoppatum, V. Srimaneepong, Parametric analysis of wavelength-dependent laser heating in skin tissue using coupled light transport and DPL-based thermoelastic models, Case Stud. Therm. Eng. (2025) 106568, https://doi.org/10.1016/j.csite.2025.106568.
[22] D.D.M. Ho, R. London, G.B. Zimmerman, D.A. Young, Laser-tattoo removal—a study of the mechanism and the optimal treatment strategy via computer simulations, Lasers Surg. Med. 30 (2002) 389–397, https://doi.org/10.1002/lsm.10065.
[23] A. Humphries, T.S. Lister, P.A. Wright, M.P. Hughes, Finite element analysis of thermal and acoustic processes during laser tattoo removal, Lasers Surg. Med. 45 (2013) 108–115, https://doi.org/10.1002/lsm.22107.
[24] A. Humphries, T.S. Lister, P.A. Wright, M.P. Hughes, Determination of the thermal and physical properties of black tattoo ink using compound analysis, Lasers Med. Sci. 28 (2013) 1107–1112, https://doi.org/10.1007/s10103-012-1198-9.
[25] C. Liu, R. Shi, M. Chen, D. Zhu, Quantitative evaluation of enhanced laser tattoo removal by skin optical clearing, J. Innov. Opt. Health Sci. 8 (2015) 1541007, https://doi.org/10.1142/S1793545815410072.
[26] K.J. Ahn, B.J. Kim, S.B. Cho, Simulation of laser-tattoo pigment interaction in a tissue-mimicking phantom using q-switched and long-pulsed lasers, Skin Res. Technol. 23 (2017) 376–383, https://doi.org/10.1111/srt.12346.
[27] K.J. Ahn, Z. Zheng, T.R. Kwon, B.J. Kim, H.S. Lee, S.B. Cho, Pattern analysis of laser-tattoo interactions for picosecond- and nanosecond-domain 1,064-nm neodymium-doped yttrium-aluminum-garnet lasers in tissue-mimicking phantom, Sci. Rep. 7 (2017) 1533, https://doi.org/10.1038/s41598-017-01724-1.
[28] L. Izikson, W. Farinelli, F. Sakamoto, Z. Tannous, R.R. Anderson, Safety and effectiveness of black tattoo clearance in a pig model after a single treatment with a novel 758 nm 500 picosecond laser: a pilot study, Lasers Surg. Med. 42 (2010) 640–646, https://doi.org/10.1002/lsm.20942.
[29] R. Zhang, W. Verkruysse, G. Aguilar, J.S. Nelson, Comparison of diffusion approximation and Monte Carlo based finite element models for simulating thermal responses to laser irradiation in discrete vessels, Phys. Med. Biol. 50 (2005) 4075, https://doi.org/10.1088/0031-9155/50/17/011.
[30] J. Saemathong, N. Pannucharoenwong, V. Mongko, S. Vongpradubchai, P. Rattanadecho, Analyzing two laser thermal energy calculation equations: a comparison of beer-Lambert's law and light transport equation, Eng. Sci. 24 (2023) 912, https://doi.org/10.30919/es912.
[31] H.H. Pennes, Analysis of tissue and arterial blood temperatures in the resting human forearm, J. Appl. Physiol. 1 (1948) 93–122, https://doi.org/10.1152/jappl.1948.1.2.93.
[32] D. Yang, M.C. Converse, D.M. Mahvi, J.G. Webster, Expanding the bioheat equation to include tissue internal water evaporation during heating, IEEE Trans. Biomed. Eng. 54 (2007) 1382–1388, https://doi.org/10.1109/TBME.2007.890740.
[33] S.L. Jacques, Optical properties of biological tissues: a review, Phys. Med. Biol. 58 (2013) R37, https://doi.org/10.1088/0031-9155/58/11/R37.
[34] A. Paul, A. Paul, Thermomechanical analysis of a triple layered skin structure in presence of nanoparticle embedding multi-level blood vessels, Int. J. Heat Mass Transf. 148 (2020) 119076, https://doi.org/10.1016/j.ijheatmasstransfer.2019.119076.
[35] A. Lorgeou, Y. Perrillat, N. Gral, S. Lagrange, J.P. Lacour, T. Passeron, Comparison of two picosecond lasers to a nanosecond laser for treating tattoos: a prospective randomized study on 49 patients, J. Eur. Acad. Dermatol. Venereol. 32 (2018) 265–270, https://doi.org/10.1111/jdv.14492.
[36] E.F. Bernstein, K.T. Schomacker, L.D. Basilavecchio, J.M. Plugis, J.D. Bhawalkar, A novel dual-wavelength, nd: YAG, picosecond-domain laser safely and effectively removes multicolor tattoos, Lasers Surg. Med. 47 (2015) 542–548, https://doi.org/10.1002/lsm.22391.
[37] E.V. Ross, G. Naseef, C. Lin, M. Kelly, N. Michaud, T.J. Flotte, R.R. Anderson, Comparison of responses of tattoos to picosecond and nanosecond q-switched neodymium: YAG lasers, Arch. Dermatol. 134 (1998) 167–171, https://doi.org/10.1001/archderm.134.2.167.
[38] M.S. Patterson, B. Chance, B.C. Wilson, Time resolved reflectance and transmittance for the noninvasive measurement of tissue optical properties, Appl. Opt. 28 (1989) 2331–2336, https://doi.org/10.1364/AO.28.002331.
[39] W. Kwan, M. Li, R. Lourdhurajan, C. Wang, Treatment guidelines for the picoway laser system in skin of color: picosecond laser therapy for benign pigmented lesions, Pract. Dermatol. (2019) 2–7.
[40] X. Du, H. Zhou, Z. Wang, et al., Comparative study of 1064 nm nanosecond, 1064 nm picosecond, 755 nm, and 595 nm lasers for tattoo removal: an essential role by macrophage, Lasers Surg. Med. 54 (2022) 737–746, https://doi.org/10.1002/lsm.23535.
[41] C. Xiao, X. Sang, D. Li, et al., Aiming to personalized laser therapy for nevus of ota: melanin distribution dependent parameter optimization, Lasers Med. Sci. 38 (2023) 10, https://doi.org/10.1007/s10103-022-03673-2.
[42] C. Deng, D. Li, B. Chen, et al., Laser parameter optimization for nevus of ota using a local non-equilibrium three-temperature heat transfer model, Int. J. Therm. Sci. 219 (2026) 110221, https://doi.org/10.1016/j.ijthermalsci.2025.110221.
[43] Y. Shimojo, T. Nishimura, H. Hazama, et al., Incident fluence analysis for 755-nm picosecond laser treatment of pigmented skin lesions based on threshold fluences for melanosome disruption, Lasers Surg. Med. 53 (2021) 1096–1104, https://doi.org/10.1002/lsm.23391.
[44] A.G. Shubnyy, V.S. Zhigarkov, V.I. Yusupov, A.P. Sviridov, Laser bleaching of tattoos: a new approach, Quant. Electron. 51 (2021) 8–16, https://doi.org/10.1070/qel17484.